Electronic Supplementary Material (ESI) for Soft Matter.
This journal is © The Royal Society of Chemistry 2023

Supporting Information for:

Coupled bond dynamics alters relaxation in polymers with multiple intrinsic dissociation rates

Robert J. Wagner[1] and Franck J. Vernerey[2*]

[1]Sibley School of Mechanical & Aerospace Engineering, Cornell University, Upson Hall, 130 Hoy Rd, Ithaca, NY 14853, USA

[2]Department of Mechanical Engineering & Material Science and Engineering Program, University of Colorado Boulder, 1111 Engineering Drive, UCB 427, Boulder, CO 80309, USA

*Correspondence to Franck.Vernerey@Colorado.edu

KEYWORDS: Dynamic polymers, Hybrid networks, Discrete network model, Transient network theory, Percolation theory

I. The discrete network model

A. Network initiation and spatiotemporal normalization

The number of nodes, $\mathcal{N} = 400$, comprising each simulated network in this study was set based according to the domain size convergence findings of **Fig. S1**. First, a 2D volume element (VE) was defined with its center at Cartesian coordinates $\boldsymbol{X} = [0,0]$ and square dimensions $L = (\mathcal{N}/\rho)^{0.5}$. Here, ρ is a tuning parameter with units of [length]$^{-2}$ used to modulate the domain density until a roughly zero stress state occurred once steady state bond dynamics were reached. This occurred when tensile entropic chain forces were approximately equilibrated with repulsive volume exclusion forces, both of which depend on the nominal node spacing. Nodes were initially seeded into the VE using a Poisson point process. To impart the networks with both stable and dynamic bonds, each node was then designated as one of three types: (i) a universal crosslinker, (ii) a stable bond crosslinker, or (iii) a dynamic bond crosslinker. This was done to mimic the composition of networks such as the hydrogels investigated by (Richardson, et al. 2019). Universal crosslinkers were permitted to bond with either stable or dynamic crosslinkers (to form stable or dynamic bonds, respectively). However, stable crosslinkers were not permitted to bond with dynamic crosslinkers, and no intraspecies bonding was permitted amongst any of the three node types. The fraction of universal crosslinkers was maintained at 50%. However, the fraction of crosslinker types comprising the remaining 50% of nodes was swept over the range of 0 to 100% stable crosslinker.

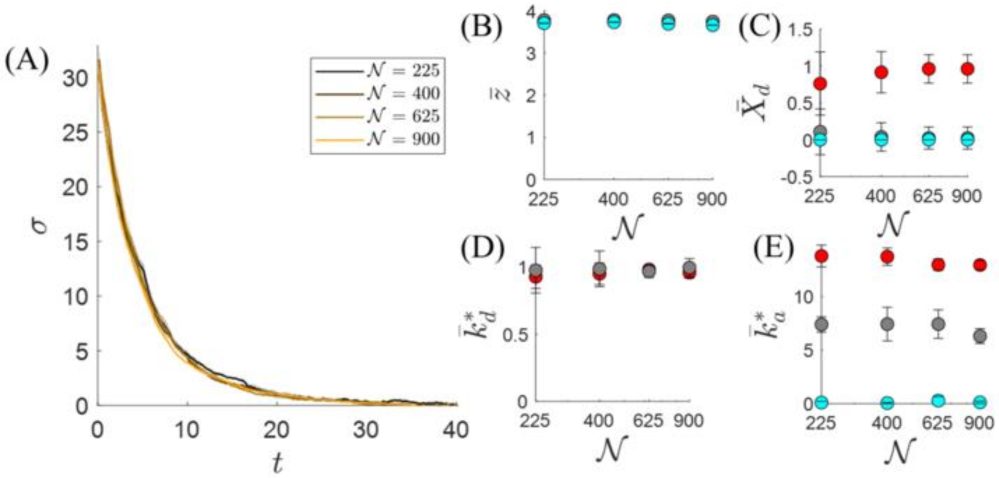

Figure S1. Domain size convergence confirmation: (A) Stress relaxation response with respect to time for the ensemble average of $n = 5$ networks containing $\mathcal{N} = \{225, 400, 625, 900\}$ nodes and $z = 4$ crosslinking sites per node. Both stress and time are given in arbitrary, but non-normalized units to illustrate that the stress response agrees for all four domain sizes. Ensemble average values of the mean **(B)** number of attachments per node, $\bar{z}$, **(C)** probability of dynamic bond percolation across the domain, $\bar{X}_d$, **(D)** detachment rate, $\bar{k}_d$, and **(E)** attachment rate, $\bar{k}_a$, all statistically converge for domains with $\mathcal{N} \geq 225$. This is confirmed for purely dynamic networks ($f = 0$, red), networks with 50% stable bonds ($f = 0.5$, grey), and purely stable networks ($f = 1$, cyan). Error bars represent standard error of the mean. Panel **(A)** confirms that the selected domain size of $\mathcal{N} = 400$ is statistically representative of the expected stress response, while **(B-E)** corroborate that it topologically representative.

Once the nodes were initially positioned and designated, they were permitted to associate and dissociate telechellically via the bond kinetics prescribed in Eqns. (1) and (2) of the manuscript. To reach steady state bond kinetics, reactions were allowed to occur (without applying any deformation to the VE) until a steady state coordination number and end-to-end chain distribution were reached. To ensure ample temporal resolution, the discretized timestep, Δt, was set at least two orders of magnitude smaller than the bond dissociation timescale, k_d^{-1}. After every reconfiguration step, the networks were equilibrated per Eqns. (3)-(6) of the manuscript. Note that the timescale of the discrete network model is in arbitrary units of time. Therefore, all values of k_d reported in the model are normalized by the central value investigated such that the normalized decadic input range is $k_d \in \{0.01, 0.1, 1, 10, 100\}$.

B. Rouse sub-diffusive scaling for bond association

The sub-diffusive Rouse model for tethered stickers' diffusion is adapted from (Stukalin, et al., 2013), which posits that the means-squared displacement of a danglin chain's end scales as:

$$\langle \Delta r^2 \rangle \approx b^2 \left(\frac{t}{\tau_0}\right)^{\frac{1}{2}}. \tag{S1}$$

where b is the Kuhn length size and τ_0 is the time it takes a monomer to diffuse distance b. Based on this, the 2D exploratory area undergone in time t is simply $\langle \Delta r^2 \rangle$. Following (Stukalin, et al., 2013), we take the distance between open crosslinks as $r_{open} \approx c_{open}^{-1/D}$, where c_{open} is the open sticker concentration and D is the model's dimensionality ($D = 2$ for the discrete model). In the discrete model, the open sticker spacing, r_{open}, is coarsely, yet directly estimated on a pair-wise basis as the distance, d, between two nodes containing open stickers. Through (S1), the time, τ_{open}, it takes an open sticker to traverse from one neighboring open sticker to another (i.e., to travel distance r_{open}) can be estimated as:

$$r_{open} \approx d \approx \left[b^2 \left(\frac{\tau_{open}}{\tau_0}\right)^{\frac{1}{2}}\right]^{\frac{1}{2}}. \tag{S2}$$

Solving (S2) for τ_{open} gives the renormalized open sticker lifetime as:

$$k_a^{-1} = \tau_{open} \approx \tau_0 \left(\frac{d}{b}\right)^4, \tag{S3}$$

where k_a is the effective attachment rate, and the effects of open sticker concentration are captured through d, which is measured explicitly in the discrete model.

C. Applied loading history

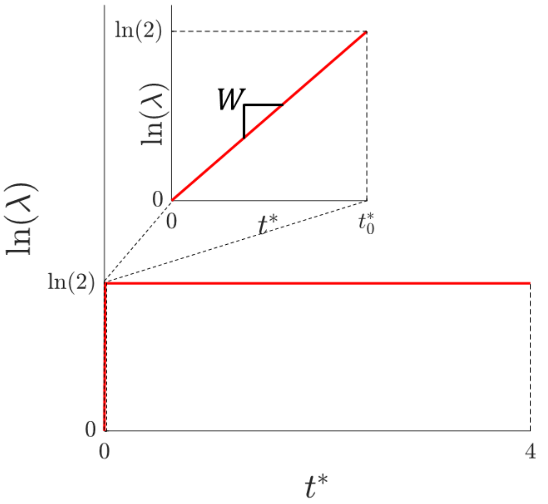

Figure S2. Applied Loading History: True strain, $\ln \lambda$, is plotted with respect to normalized time, $t^* = tk_d$. The inset displays $\ln \lambda$ versus t^* (with a significantly dilated time axis) to illustrate the definition of $\dot{\varepsilon}/k_d = \ln(\lambda)\ /t^*$, which was set to 100 to approximate elastic loading.

C. Parametric space

Detailed parametric values and sweeping ranges for the discrete network model are provided in **Tables S1** and **S2**, respectively.

Table S1. Detailed parametric definitions and values for the discrete network model.

Parameter	Definition	Swept Values	Reason for Value
$\mathcal{N}$	Nodes per domain	400	Set to ensure convergence of stress response with respect to increasing domain size per (Wagner, et al. 2021)
ζ	Normalization length scale	$\sqrt{\mathcal{N}}$	Set such that each node occupies on order of 1-unit length^2
L^*	Initial square domain dimensions	$\zeta\rho^{-0.5}$	Set such that each node occupies on order of 1-unit length^2
ρ^*	Scaling coefficient to adjust domain density	1.78	Set to equilibrate entropic tensile forces with volume exclusion in initial networks.
τ_0	Kuhn segment diffusion timescale	1×10^{-9}	Preserved from (Wagner, et al. 2021)
k_bT	Normalized thermal energy scale	5×10^{-2}	
N	Kuhn segments per chain	700	
b^*	Normalized Kuhn length	5×10^{-3}	
E	Force scaling coefficient to adjust repulsion magnitude	1.25	
γ	Scaling coefficient to adjust repulsion stiffness	2	
R^*	Normalized volume exclusion cutoff distance	Nb^*	
η^*	Normalized numerical damping viscosity	1.5×10^{-4}	
Δt^*	Discretized time	$\Delta t^* < 0.01 \cdot k_d^{-1}$	Set to ensure ample temporal resolution during reconfiguration

Table S2. Detailed sweeping ranges of free parameters of the discrete network model.

Parameter	Definition	Swept Values
f	Fraction of stable bonds.	$\{0,10,\ldots 90,100\}\%$
k_d	Normalized detachment rate	$\{0.01,0.1,1,10,100\}$
z	Functionality (i.e., no. of potential bonds per crosslink)	$\{4,8\}$

II. Transient Network Theory Derivations

A. Initial loading and stress normalization

From the manuscript, the simple rule of mixture gives:

$$\boldsymbol{\sigma} = k_b T(c^s \boldsymbol{b} + c^d \boldsymbol{\mu}) + \pi \boldsymbol{I}, \tag{S4}$$

where, $c^s = cp^s f$ and $c^d = cp^d(1-f)$. We aim to normalize this stress by the peak stress, which occurs at the time of load rate cessation. Recalling that $\boldsymbol{\mu}$ evolves according to Eqn. (8) of the manuscript:

$$\dot{\boldsymbol{\mu}} = \boldsymbol{L}\boldsymbol{\mu} + \boldsymbol{\mu}\boldsymbol{L}^T - k_d(\boldsymbol{\mu} - \boldsymbol{I}). \tag{S5}$$

and given $\dot{\varepsilon} \gg k_d$, the rightmost term in (S5) approaches zero during loading, leaving:

$$\dot{\boldsymbol{\mu}} = \boldsymbol{L}\boldsymbol{\mu} + \boldsymbol{\mu}\boldsymbol{L}^T, \tag{S6}$$

where $\boldsymbol{L} = \dot{\boldsymbol{F}}\boldsymbol{F}^{-1}$, $\dot{\boldsymbol{F}} = \partial \boldsymbol{F}/\partial t$, and $\boldsymbol{F} = \text{diag}(\lambda^{-1}, \lambda)$. For uniaxial extension occurring in the second principal direction, we are concerned with the evolution of μ_{22}, which evolves according to:

$$\frac{\partial \mu_{22}}{\partial t} = 2\mu_{22}\lambda^{-1}\frac{\partial \lambda}{\partial t}. \tag{S7}$$

Integrating both sides with the condition $\mu_{22}(\lambda = 1) = 1$ gives:

$$\mu_{22} = \lambda^2 = b_{22}, \tag{S8}$$

for fast loading. Substituting (S8) into (S4) gives the stress component in the principal direction of stretch as:

$$\sigma_{22}^{max} = ck_b T[p^s f + p^d(1-f)]\lambda^2 + \pi. \tag{S9}$$

Similar analysis in the direction normal to stretch gives:

$$\sigma_{11}^{max} = ck_b T[p^s f + p^d(1-f)]\lambda^{-2} + \pi, \tag{S10}$$

with the added traction-free boundary condition that $\sigma_{11} = 0$. Solving for π in (S10) and substituting into (S9) gives:

$$\sigma_{22}^{max} = ck_b T[p^s f + p^d(1-f)]\left(\lambda^2 - \frac{1}{\lambda^2}\right). \tag{S11}$$

B. Stress relaxation

To induce stress relaxation, the strain rate is removed (i.e., $\boldsymbol{L} = \boldsymbol{0}$) such that (S5) becomes:

$$\dot{\boldsymbol{\mu}} = -k_d(\boldsymbol{\mu} - \boldsymbol{I}). \tag{S12}$$

Taking the time at which stress relaxation begins as the reference time, $t = 0$, and solving (S12) for the principal components of $\boldsymbol{\mu}$ gives:

$$\mu_{11} = (\mu_{11}^0 + 1)e^{-k_d t} - 1, \tag{S13}$$

and:

$$\mu_{22} = (\mu_{22}^0 + 1)e^{-k_d t} - 1, \tag{S14}$$

where, from (S8), $\mu_{11}^0 = \lambda^{-2}$ and $\mu_{22}^0 = \lambda^2$ since $\dot{\varepsilon} \gg k_d$ during initial loading. Substituting (S13) and (S14) into (S4) gives the principal components of stress as:

$$\sigma_{11} = ck_bT\{p^s f\lambda^{-2} + p^d(1-f)[(\lambda^{-2}+1)e^{-k_d t} - 1]\} + \pi, \tag{S15}$$

and:

$$\sigma_{22} = ck_bT\{p^s f\lambda^{2} + p^d(1-f)[(\lambda^{2}+1)e^{-k_d t} - 1]\} + \pi. \tag{S16}$$

Applying the traction-free boundary condition (i.e., $\sigma_{11} = 0$), solving for π, and substituting π into (S16) gives the principal component of stress in the extensile direction as:

$$\sigma_{22} = ck_bT\left(\lambda^2 - \frac{1}{\lambda^2}\right)\{p^s f + p^d(1-f)e^{-k_d t}\}. \tag{S17}$$

Finally, normalizing (S17) by (S11) provides the normalized tensile stress as:

$$\sigma^* = [p^s f + p^d(1-f)e^{-k_d t}][p^s f + p^d(1-f)]^{-1}. \tag{S18}$$

C. Incorporating the coupling parameter

Supposing that some fraction of stable bonds, $1-\xi$, are sufficiently jammed by surrounding crosslinks or bonded into a stable bond scaffold such that they affinely follow the global deformation gradient, $\boldsymbol{F}$, without relaxation (while the remaining fraction, ξ, can relax into lower energy conformations), then we may rewrite Eqn. (S4) as:

$$\boldsymbol{\sigma} = ck_bT[p^s f(1-\xi)\boldsymbol{b} + p^s f\xi\boldsymbol{\mu} + p^d(1-f)\boldsymbol{\mu}] + \pi\boldsymbol{I}. \tag{S19}$$

As a simple first assumption, we have invoked that the rate of stable bond relaxation due to conformational change is synonymous with that of bond dissociation of neighboring dynamic bonds (i.e., k_d) through $\boldsymbol{\mu}$. Thus, during elastic loading, $\boldsymbol{\mu} \to \boldsymbol{b}$ and (S19) reverts to Eqn. (9). As before, the condition that $\sigma_{11} = 0$, along with the definitions of $\boldsymbol{\mu}$ from (S13) and (S14) are used to solve for π, which then allows that component of stress in the extensile direction be written:

$$\sigma_{22} = ck_bT\left(\lambda^2 - \frac{1}{\lambda^2}\right)[p^s f(1-\xi) + p^s f\xi e^{-k_d t} + p^d(1-f)e^{-k_d t}]. \tag{S20}$$

Once again normalizing (S20) by (S11) gives the normalized tensile stress as:

$$\sigma^* = [p^s f(1-\xi) + p^s f\xi e^{-k_d t} + p^d(1-f)e^{-k_d t}][p^s f + p^d(1-f)]^{-1}. \tag{S21}$$

D. Hybrid networks with two dissociation timescales

Supposing that a hybrid network is comprised of two different types of dynamic bonds with two distinct dissociation timescales, k_β^{-1} and k_α^{-1}, such that that the former types of bonds detach significantly slower than the latter (i.e., $k_\beta \ll k_\alpha$). Then Eqn. (11) may be rewritten as:

$$\boldsymbol{\sigma} = ck_bT\left[p^\beta f(1-\xi)\boldsymbol{\mu}^\beta + p^\beta f\xi\boldsymbol{\mu}^\alpha + p^\beta(1-f)\boldsymbol{\mu}^\alpha\right] + \pi\boldsymbol{I}. \tag{S22}$$

where $\boldsymbol{\mu}^{\alpha}$ and $\boldsymbol{\mu}^{\beta}$ and are the conformation tensors of the chains adjoined by more and less dynamic bonds, respectively. During stress relaxation, these conformation tensors evolve according to $\dot{\boldsymbol{\mu}}^{\beta} = -k_{\beta}\left(\boldsymbol{\mu}^{\beta} - \boldsymbol{I}\right)$ and $\dot{\boldsymbol{\mu}}^{\alpha} = -k_{\alpha}\left(\boldsymbol{\mu}^{\alpha} - \boldsymbol{I}\right)$. In (S22), we have assumed that the coupled stress term relaxes at the faster dissociation rate of the more dynamic bonds (i.e., at a rate k_{α}) since the dissociation of the more stable bonds is considerably slower (i.e., $k_{\beta} \ll k_{\alpha}$).

Here we apply simple shear conditions to approximate the parallel plate rheometry conducted by (Richardson, et al. 2019) for which:

$$\boldsymbol{F} = \begin{bmatrix} 1 & \gamma & 0 \\ 0 & 1 & 0 \\ 0 & 0 & 1 \end{bmatrix}, \tag{S23}$$

and:

$$\boldsymbol{L} = \begin{bmatrix} 0 & \dot{\gamma} & 0 \\ 0 & 0 & 0 \\ 0 & 0 & 0 \end{bmatrix}, \tag{S24}$$

where γ is the peak shear strain and $\dot{\gamma}$ is the shear rate. Again, during loading ($\dot{\gamma} \gg k_{\alpha}$ and $\dot{\gamma} \gg k_{\beta}$), $\boldsymbol{\mu}_{\beta} \rightarrow \boldsymbol{b}$ and $\boldsymbol{\mu}_{\alpha} \rightarrow \boldsymbol{b}$, giving (S22) as:

$$\boldsymbol{\sigma} = ck_bT\left[p^{\beta}f + p^{\alpha}(1-f)\right]\boldsymbol{b} + \pi\boldsymbol{I}. \tag{S25}$$

Solving for $\boldsymbol{b} = \boldsymbol{F}\boldsymbol{F}^{T}$ and substituting into (S25) gives the peak shear stress as:

$$\sigma_{12} = ck_bT\left[p^{\beta}f + p^{\alpha}(1-f)\right]\gamma. \tag{S26}$$

During stress relaxation (i.e., $\boldsymbol{L} = \boldsymbol{0}$), given relatively small shear strain ($\gamma \sim 0.1$) then the principal orientation of chain stretch remains relatively unaffected, and we may uphold the general relation (S26) for both dynamic bond types (i.e., the shear components may be written $\mu^{\beta} \approx \exp\left(-k_{\beta}t\right)$ and $\mu^{\alpha} \approx \exp\left(-k_{\alpha}t\right)$). Therefore, the shear component of stress from (S22) may be written as follows during stress relaxation:

$$\sigma_{12} = ck_bT\left[p^{\beta}f(1-\xi)e^{-k_{\beta}t} + p^{\beta}f\xi e^{k_{\alpha}t} + p^{\alpha}(1-f)e^{-k_{\alpha}t}\right]\gamma. \tag{S27}$$

Normalizing (S27) by the peak shear stress from (S26) gives:

$$\sigma^{*} = \begin{bmatrix} p^{\beta}f(1-\xi)e^{-k_{\beta}t} + p^{\beta}f\xi e^{-k_{\alpha}t} + \cdots \\ \ldots p^{\alpha}(1-f)e^{-k_{\alpha}t} \end{bmatrix}\left[p^{\beta}f + p^{\alpha}(1-f)\right]^{-1}. \tag{S28}$$

E. Bond Lifetime Renormalization and Bell's Theory

The experimental stress relaxation data provided by (Richardson, et al. 2019) exhibits a variable relaxation rate with faster relaxation at shorter timescales. A possible origin of slower long-tail relaxation is that of bond lifetime renormalization (Stukalin, et al. 2013), which suggests that the emergent relaxation rate of a transient polymer network is not necessarily the intrinsic bond dissociation rate, τ_i^{-1}, but rather the rate at which bonds detach from one configuration and reattach into another. Thus, the effective or "renormalized" bond lifetime governing dissipation is actually:

$$\tau_i^{rn} \approx J(\tau_{open})\tau_i + \tau_{open}, \tag{S29}$$

where $J(t)$ is the number of instances a given bonding pair breaks and reattaches into the same configuration over the duration of time, t, and τ_{open} is the amount of time it takes for an unbound end group or "sticker" to diffuse the distance, r_{open}, between adjacent open stickers. Note that $r_{open} \approx c_{open}^{-1/3}$ where c_{open} is the open sticker concentration. Prescribing Rouse sub-diffusive behavior, then the mean-square displacement of a sticker may be written as:

$$\langle \Delta r^2(t) \rangle \approx b^2 \left(\frac{t}{\tau_0}\right)^{1/2}, \tag{S30}$$

where b is the Kuhn length or length scale of a sticker, and τ_0 is the time it takes a sticker to diffuse a distance b. Therefore, the time of diffusion over distance r_{open} may be estimated from:

$$r_{open} \approx \langle \Delta r^2(\tau_{open}) \rangle^{1/2} \approx b \left(\frac{t}{\tau_0}\right)^{1/4}, \tag{S31}$$

giving:

$$\tau_{open} \approx \tau_0 \left(\frac{r_{open}}{b}\right)^4. \tag{S32}$$

Supposing there is no long-range attraction between binding sites, then a bond reforms when two open stickers diffuse into the same volume at the length scale of a Kuhn segment, b. Therefore, the mean number of times a bond will break and reform into the same configuration over $n(t)$ steps (of duration τ_0) may be estimated as the number of times they diffuse into the same explored space. Thus:

$$J(t) \approx \frac{n(t)b^3}{\langle \Delta r^2(t) \rangle^{3/2}}, \tag{S33}$$

where $\langle \Delta r^2(t) \rangle^{3/2} \cdot b^{-3}$ is the approximate volume explored during t. Therefore, the number of repeated binding instances occurring in time τ_{open} is approximately:

$$J(\tau_{open}) \approx \frac{r_{open}}{b}, \tag{S34}$$

where we have applied the definition of $\langle \Delta r^2(\tau_{open}) \rangle$ through (S30), substituted τ_{open}/τ_0 for $n(\tau_{open})$, and simplified the expression. Substituting Eqns. (S32) and (S34), as well as the force-adjusted Arrhenius-like relation from Eqn. (15) into (S29) gives the renormalized lifetime of bond type i as:

$$\tau_i^{rn} \approx \tau_0 \left(\frac{r_{open}}{b}\right) \left[K_i^0 \exp\left(-\frac{3\Delta x}{\sqrt{N}b}\bar{\lambda}\right) + \left(\frac{r_{open}}{b}\right)^3\right]. \tag{S35}$$

where $\bar{\lambda}$ is the magnitude of mean chain stretch, and Δx is distance from the equilibrium bond length to the activation barrier. The exponential prefactor $K_i^0 = \exp(\varepsilon_i/k_bT)$ (where k_b is the Boltzmann constant, T is temperature) is a dimensionless parameter that encapsulates the intrinsic bond activation energy, ε_i, and defines the mean bond lifetime ($K_i^0\tau_0$) of a Gaussian chain in an equilibrated network (i.e., when $\bar{\lambda} \to 1$).

At this stage, we must distinguish between the bond types, aHz and bHz, as these express different open sticker concentrations, which are taken as proportionate to the overall open sticker concentration, c_{open}, and the respective fraction of each bond type, giving $c_\alpha \approx c_{open}(1-f)$ for aHz and $c_\beta \approx c_{open}f$ for bHz. As such, the distances between open stickers for each respective population may be written as:

$$r_{open}^{\alpha} \approx \left[c_{open}(1-f)\right]^{-1/3}, \tag{S36}$$

and:

$$r_{open}^{\beta} \approx \left(c_{open}f\right)^{-1/3}, \tag{S37}$$

such that the renormalized lifetimes of each bond type are:

$$\tau_\alpha^{rn} \approx \frac{\tau_0}{\left[c_{open}^*(1-f)\right]^{1/3}}\left[K_\alpha^0 \exp\left(-\frac{3\Delta x}{\sqrt{N}b}\bar{\lambda}\right) + \frac{1}{c_{open}^*(1-f)}\right]. \tag{S38}$$

and:

$$\tau_\beta^{rn} \approx \frac{\tau_0}{\left(c_{open}^*f\right)^{1/3}}\left[K_\beta^0 \exp\left(-\frac{3\Delta x}{\sqrt{N}b}\bar{\lambda}\right) + \frac{1}{c_{open}^*f}\right]. \tag{S39}$$

where $c_{open}^* = c_{open}b^3$ is the open bond concentration normalized by the characteristic Kuhn volume, b^3.

To utilize (S38) and (S39) given the normalized stress data provided by (Richardson, et al. 2019) we must relate the force in a single chain to the global stress state measured in experiments. Following the virial formulation (Wagner, et al. 2022), the network's ensemble Cauchy stress may be computed from the integral over the chain space, Ω, as:

$$\boldsymbol{\sigma} = \frac{3k_bTc}{2\mathcal{N}}\int_V(\boldsymbol{\lambda} \otimes \boldsymbol{\lambda}). \tag{S40}$$

where $\mathcal{N}/c$ is the total volume of a population of $\mathcal{N}$ chains at a concentration of c. Supposing that stretch is homogenously distributed throughout the network and normally distributed about the mean, then the local stretch state in a single chain may be well-represented by the mean stretch, $\bar{\boldsymbol{\lambda}}$, such that (Vernerey, et al. 2017):

$$\boldsymbol{\sigma} \approx \frac{3}{2}ck_bT\left(\bar{\boldsymbol{\lambda}} \otimes \bar{\boldsymbol{\lambda}}\right). \tag{S41}$$

Therefore, the shear component of stress measured in experiments may be approximated as:

$$\sigma_{12} \approx 3ck_bT\bar{\lambda}^2\sin(2\gamma), \tag{S42}$$

where – given simple shear conditions – we have assumed no radial stretch (i.e., $\lambda_3 =$

1), and invoked that $\lambda_1 = \bar{\lambda}\sin\gamma$, $\lambda_2 = \bar{\lambda}\cos\gamma$, and $\bar{\lambda} = \sqrt{1+\gamma^2}$ for the strain magnitude, γ. Normalizing (S42) by (S27) gives the normalized stress as:

$$\sigma^* \approx \frac{3\bar{\lambda}^2\sin(2\gamma)}{[p^\beta f + p^\alpha(1-f)]\gamma}, \tag{S43}$$

where the fractions of attached aHz or bHz bonds are assumed roughly equal as $p^\alpha \approx p^\beta \approx 1 - c^*_{open}/c^*$, and $c^* = cb^3$ is the normalized concentration of all attached chains.

Solving for $\bar{\lambda}$ in (S43), substituting into (S38) and (S39), and then simplifying gives the renormalized bond lifetimes as:

$$\tau_\alpha^{rn} \approx \frac{\tau_0}{[c^*_{open}(1-f)]^{1/3}}\left[K_\alpha^0 \exp\left(-\sqrt{\frac{\sigma^*}{\sigma_0^*}}\right) + \frac{1}{c^*_{open}(1-f)}\right], \tag{S44}$$

and:

$$\tau_\beta^{rn} \approx \frac{\tau_0}{(c^*_{open}f)^{1/3}}\left[K_\beta^0 \exp\left(-\sqrt{\frac{\sigma^*}{\sigma_0^*}}\right) + \frac{1}{c^*_{open}f}\right]. \tag{S45}$$

Here σ_0^*, is a stress sensitivity parameter given by:

$$\sigma_0^* = \left(\frac{b}{\Delta x}\right)^2 \frac{N\sin(2\gamma)}{3p\gamma}, \tag{S46}$$

that lumps together the effects of applied strain (γ), attached chain fraction ($p = 1 - c^*_{open}/c^*$), and chain length (through N and b). Supposing a high fraction of the chains are always attached $p \sim 1$; estimating $N \approx 88$ based on the molecular weight of macromers used in experiments ($M_w = 8{,}000\ \mathrm{g\ mol^{-1}}$), the number of branches per macromer ($z = 8$), and the molar mass of ethylene glycol ($44.05\ \mathrm{g\ mol^{-1}}$) (Wagner, et al. 2022); and given an experimental strain of $\gamma = 0.1$, then the normalized bond activation length may be estimated by:

$$x^* = \frac{\Delta x}{b} = \sqrt{\frac{N\sin(2\gamma)}{3p\gamma}\sigma_0^*} \approx 10.8\sqrt{\sigma_0^*}. \tag{S47}$$

Inverting (S44) and (S45) provides the characteristic relaxation times associated with each bond type as expressed in Eqns. (16) and (17) of the manuscript.

$$k_\alpha \approx \frac{[c^*_{open}(1-f)]^{\frac{1}{3}}}{\tau_0}\left[K_\alpha^0 \exp\left(-\sqrt{\frac{\sigma^*}{\sigma_0^*}}\right) + \frac{1}{c^*_{open}(1-f)}\right]^{-1}, \tag{S48}$$

and:

$$k_\beta \approx \frac{(c^*_{open}f)^{1/3}}{\tau_0}\left[K_\beta^0 \exp\left(-\sqrt{\frac{\sigma^*}{\sigma_0^*}}\right) + \frac{1}{c^*_{open}f}\right]^{-1}. \tag{S49}$$

Using Eqns. (S28), (S48), and (S49), stress relaxation responses are computed in discretized time using an explicit forward Euler approach, with a timestep of $\Delta t = 36$ s, which was iteratively reduced (over $\Delta t \in \{360, 180, 36, 18\}$ s) until the results of the fitted parameters expressed less than a 1% change from the previous timestep size.

F. Parametric fitting

For parametric fitting, thirteen values for each parameter were sampled from a normal distribution about some mean initial guesses. The model stress was then computed for each combination of parameters, and whichever yielded the coefficient of determination closest to unity ($\min(|1-R^2|)$), was then taken as a new set of mean distribution values from which parameters were sampled. Non-physical values (e.g., $\xi > 1$, $c_{open}^{*} < 0$, etc.) were excluded from the parameter space. Note that to ensure convergence, nominal or mean values of the distributions from the previous iteration were always included when probing the stress response. Each time the mean values of the distributions yielded the lowest error, the standard deviations of the distributions were reduced by a factor of 0.97. Iteration was carried out until the coefficient of determination, $R^2 > 0.995$.

III. Extended Network Model Results & Interpretations

A. Bond Dynamics, Percolation, & the Relaxation Factor

Fig. S3 depicts the average measured bond dynamics over $n = 10$ simulations for networks with varied values of f and k_d.

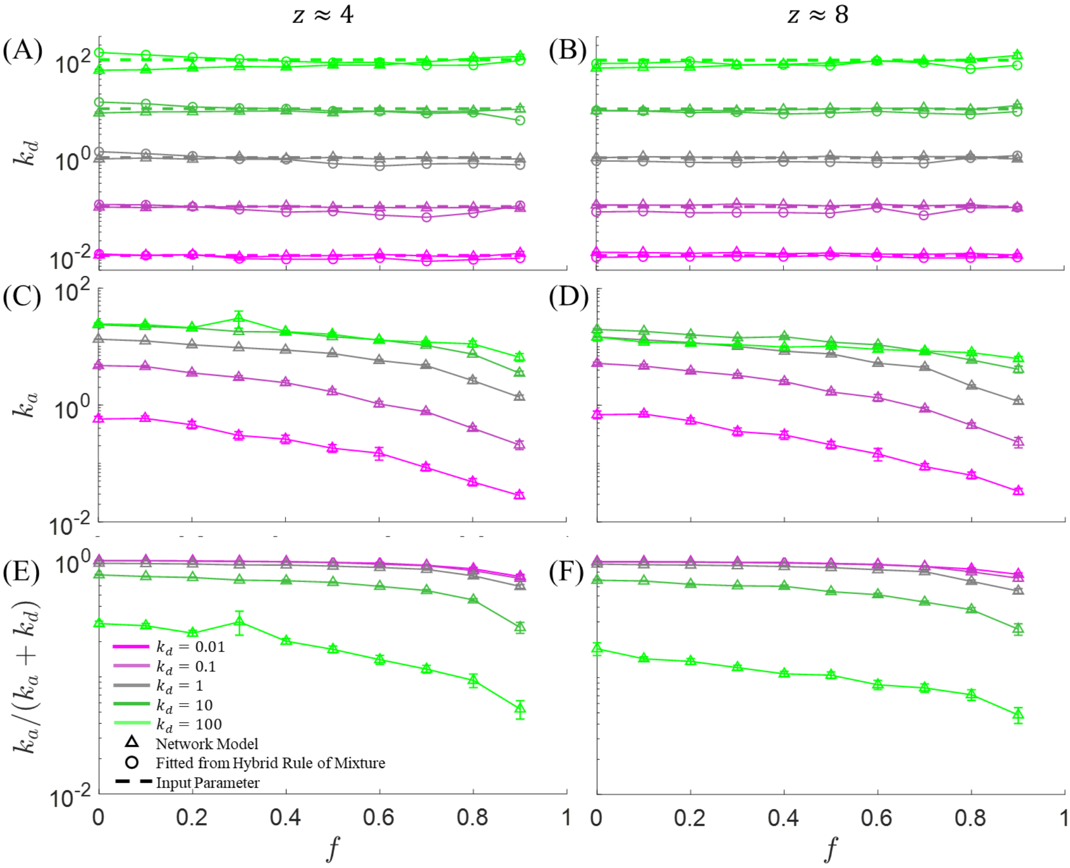

Figure S3. Bond Dynamics as Measured from Discrete Model: (A-B) To verify consistency between the two modeling approaches, Average dynamic bond dissociation rate, k_d, is plotted with respect to the stable bond fraction, f, and input value of detachment rate, k_d, when coordination is **(A)** $z = 4$ and **(B)** $z = 8$. **(C-D)** Average dynamic bond association rate, k_a, is plotted with respect to f and k_d for **(C)** $z = 4$ and **(D)** $z = 8$. **(E-F)** Steady state attached dynamic bond fraction, $p^d = k_a/(k_a + k_d)$, is plotted with respect to f and k_d for **(E)** $z = 4$ and **(F)** $z = 8$.

As expected, measured values of average k_d agree with the *a priori* values input into the discrete model. Furthermore, k_d is uncorrelated with stable bond fraction, f (**Fig. S3.A-B**) corroborating that the dissociation timescale is the same for the various curves (representing different values of f) in **Fig. 2** or **4**. In contrast, k_a is directly correlated with k_d and inversely correlated with f (**Fig. S3.C-D**). This is because open bonds may only attach to neighboring open sites within a radial distance of the maximum chain length. Since, the number of attachment opportunities at a given time scales with k_d, so too does k_a. This effect is reflected in $k_a/(k_a + k_d)$, which indicates the steady state probability that a given dynamic bond is attached (**Fig. S3.E-F**). It occurs due to a prescribed polymer diffusion timescale, τ_0, (and therefore bond association timescale) that is significantly lower than the bond dissociation timescale (i.e., $k_d \ll k_a$). While

$k_a/(k_a + k_d)$ remains close to unity and appears relatively independent of k_d when $k_d \sim 0.01$ to 10, it decreases substantially when the dissociation rate is high (e.g., $k_d \sim 100$). This suggests that the intrinsic association rate, k_a, is somewhere on the order of 10 and that discrete network results should therefore only be considered for the cases in which $k_d \lesssim 10$, exhibiting high network connectivity.

Regarding the effects of stable bond fraction on bond dynamics, increasing f reduces the number of dynamic bonding opportunities and therefore decreases the effective k_a (**Fig. S3.C-D**). Since k_a is lower for higher values of f, $k_a/(k_a + k_d)$ is as well (**Fig. S3.E-F**), which influences the probability of dynamic bond percolation as discussed below. Interestingly, coordination has negligible influence on the measured bond dynamics. However, this independence is likely contingent on the allowance of redundant bonds between neighboring nodes, which ensures that k_a is more influenced by the number and distribution of nodes (as they govern bonding opportunities) than the total number of bonds. The relative independence of k_a and k_d is also reflected by the highly similar plots of attached bond probabilities, $P^s = p^s f$, $P^d = p^d(1 - f)$, and $P = P^s + P^d$ in **Fig. S4**. However, P^d (and therefore P) is slightly smaller (i.e., there are more dangling dynamic chains) at high k_d ($k_d = 10$ or 100) and higher coordination ($z = 8$), which suggests that attachment opportunities are saturated at the higher coordination number.

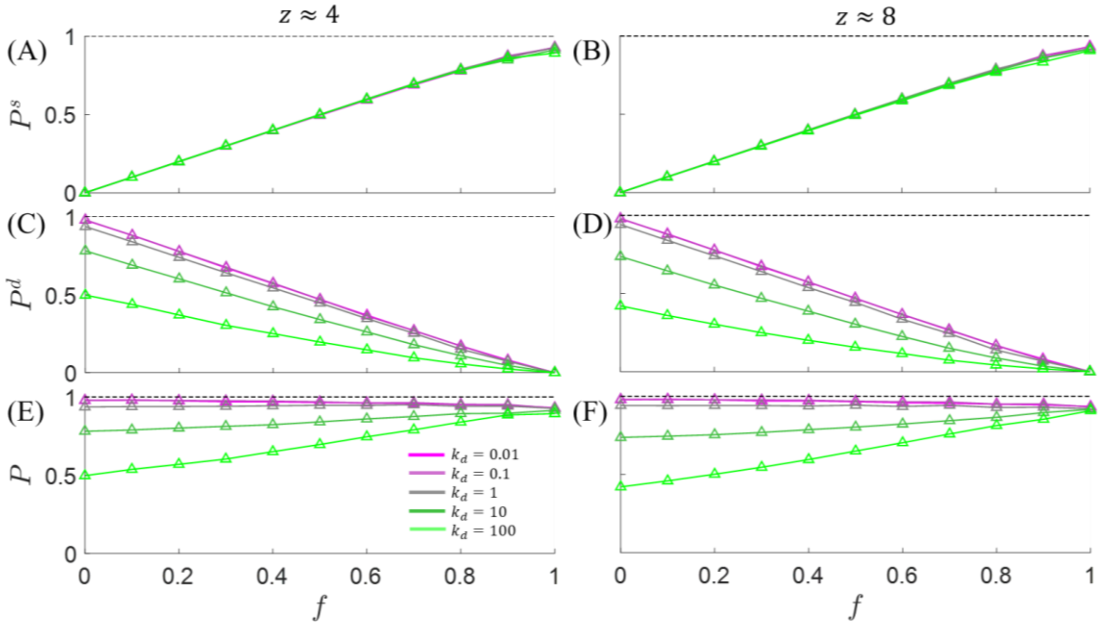

Figure S4. Bond Attachment Probabilities from Discrete Model: (A-B) The average probability that a bond is stable and attached, $P^s = fp^s$, is plotted with respect to the stable bond fraction, f, and input value of detachment rate, k_d, when maximum coordination is **(A)** $z = 4$ and **(B)** $z = 8$. **(C-D)** The average probability that a bond is dynamic, $P^2 = (1 - f)p^2$, and attached is plotted with respect to f and k_d for **(C)** $z = 4$ and **(D)** $z = 8$. **(E-F)** The probability that a given bond is attached, $P = P^s + P^d$, is plotted with respect to f and k_d for **(E)** $z = 4$ and **(F)** $z = 8$.

Fig. S5 depicts the average probabilities (over $n = 10$ simulations each) that the independent bond types form percolated networks when f and k_d are swept. **Fig. S5.A-**

B confirms that the probability of stable bond percolation is not strongly dependent on k_d. Going from $z = 4$ to $z = 8$, the stable bond percolation threshold (i.e., lowest fraction of bonds at which the networks may percolate) shifted to lower relative fractions of stable bonds, from approximately $f \sim 0.3$ to $f \sim 0.2$. Meanwhile, **Fig. S5.C-D** confirms that dynamic bond percolation is highly dependent on k_d, with higher values of k_d universally decreasing the probability that the dynamic bonds form a percolated network. Going from $z = 4$ to $z = 8$ the percolation threshold undergoes a shift from $1 - f \sim 0.3$ to $1 - f \sim 0.2$. This directly mirrors the shift observed for the stable bond percolation threshold.

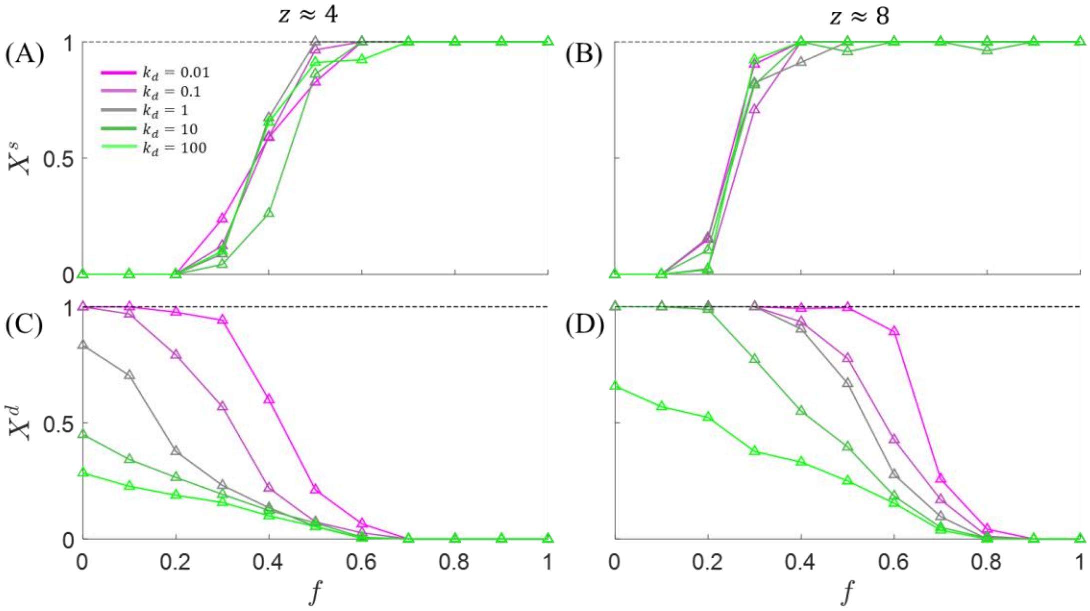

Figure S5. Decoupled Network Percolation Probabilities: (A-B) The average probability that the stable bonds independently form a percolated network, X^s, is plotted with respect to stable bond fraction, f, and input value of detachment rate, k_d, when maximum coordination is **(A)** $z = 4$ and **(B)** $z = 8$. **(C-D)** The average probability that the dynamic bonds independently form a percolated network, X^d, is plotted with respect to f and k_d for **(C)** $z = 4$ and **(D)** $z = 8$.

Fig. S6 depicts the average ($n = 10$) fitted values of $1 - \xi$, which represents the extent to which stable bonds are unable to relax, when f and k_d are swept. The scaling law given by Eqn. (13) is fitted to each discrete data set, where η represents the fraction of stable bonds that remain unable to relax in the limit $f \to 0$. Generally, η decreases as the dissociation rate increases, intuitively suggesting that higher bond dynamic beget lower fractions of topologically constrained stable bonds when $f \sim 0.1$. Notably, ξ is not well predicted by Eqn. (13) when $z = 8$, which is attributed to the fact that dynamic bonds in these networks saturate the bond attachment opportunities such that there exists a greater degree of dangling stable bonds than in the networks with $z = 4$. Consequently, this reduces the effective fraction of attached stable bonds that are unable to relax at higher stable bond concentrations (**Fig. S6.B**) below the expected asymptotic limit, $1 - \xi = f$ ($\eta \to 0$).

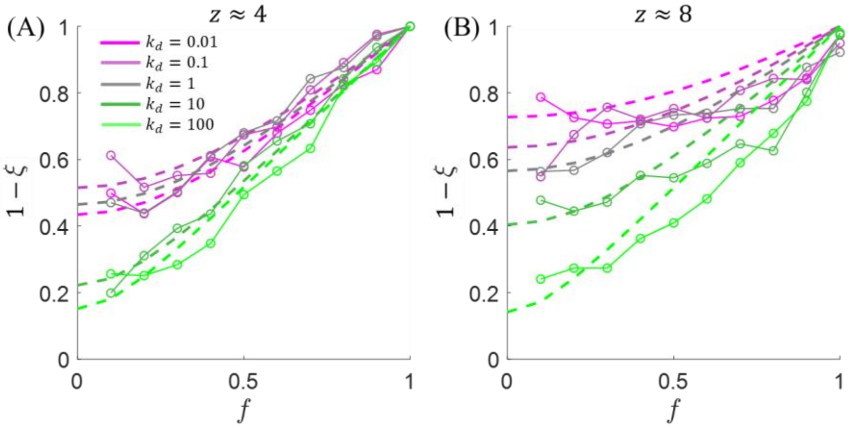

Figure S6. Effect of network coordination on stable bond relaxation: (A-B) The stable bond non-relaxation degree, $1 - \xi$, is plotted with respect to f for the ensemble average of $n = 10$ networks with **(A)** $z = 4$ and **(B)** $z = 8$.

B. Effects of Chain Length

A topologically influential parameter hypothesized to influence stable bond relaxation is the length of the chains. As such, chains with normalized lengths of $L^* = 0.5$ and $L^* = 2$ (where L^* is the contour length of a chain, Nb, normalized by the contour length of chains investigated in the main manuscript) were used to generate and test the stress relaxation of discretely modeled networks. Networks were generated and mechanically tested using the same procedure as earlier experiments (wherein $L^* = 1$). The coupled ROM was subsequently fit to the data treating ξ as a fitting parameter. Stress relaxation results for shorter and longer chains are depicted in **Fig. S7.A** and **S7.B**, respectively. While the coupled ROM can predict the stress relaxation of the networks of longer chains without significant error, it is unable to do so for the networks of shorter chains at early stages of the relaxation process during which the discrete model relaxes significantly faster than the coupled ROM predicts through k_d.

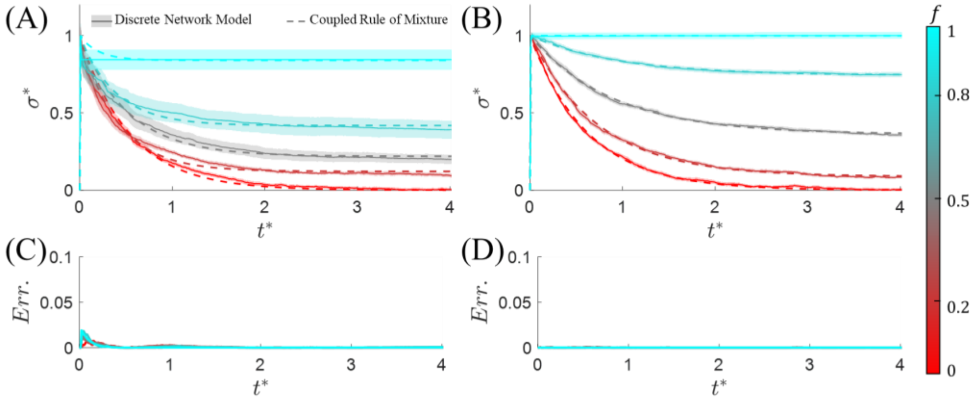

Figure S7. Fitting the coupled ROM to networks with variable chain length: (A) Normalized stress, σ^*, is plotted with respect to normalized time, t^*, for the ensemble average of $n = 10$ discrete simulations (solid curves with shaded S.E.) and as predicted by Eqn. (12) (dotted curves) when $k_d = 1$ and chain length is doubled ($L^* = 2$). **(C-D)** Absolute errors between the models' σ^* are plotted with respect to t^* for **(C)** $L^* = 0.5$ and **(D)** $L^* = 2$ (where L^* is the chain contour length normalized by the original chain length investigated).

The likely cause of this discrepancy is revealed by examining the degree of percolation in these short chain networks (**Fig. S8.A**). **Fig S8.A** indicates that even when $f = 1$, the stable bonds in the domain do not form percolated networks with 100% probability. As such, it is likely that stable bonds in short chain networks experience less entropic penalty (i.e., reduced conformational degrees of freedom) due to network structure, and are instead only constrained by steric interactions. The short timescale of relaxation that exists even for entirely stable bond networks likely results from floppy modes of cluster reconformation and indicates that these networks are not sufficiently equilibrated during loading. Here, this is a numerical artifact and indicates that for short chain networks in which inter-chain volume exclusion interactions dominate network topology, a lower residual force criterion is needed during equilibration. Alternatively, in systems with low connectivity loaded at rates exceeding the rate of floppy relaxation, another stress term governed by a shorter relaxation timescale may be necessary to include in the coupled ROM. Without this term, the coupled ROM should be applied only to percolated networks.

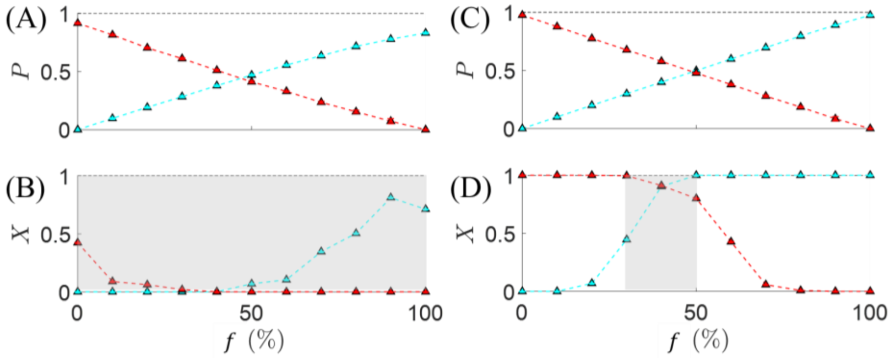

Figure S8. Effect of chain length on bond percolation: (A-B) The probability that the stable (cyan) and dynamic (red) bonds independently form geometrically percolated networks (X^s and X^d) are plotted with respect to f for **(A)** $L^* = 0.5$ and (B) $L^* = 2$ when $z = 4$ and $k_a = 1$. **(G-H)** The regions shaded grey demark transition zones wherein simultaneous percolation of both bond types is possible ($X > 0$).